IEEE Journal of Microwaves

Received 3 December 2021; revised 16 February 2022 and 23 February 2022; accepted 23 February 2022. Date of publication 28 March 2022; date of current version 7 April 2022.

Digital Object Identifier 10.1109/JMW.2022.3154886

Coherent Measurements of a Multistatic MIMO Radar Network With Phase Noise Optimized Non-Coherent Signal Synthesis

ANDRÉ DÜRR [1] (Graduate Student Member, IEEE), DENNIS BÖHM [2], DOMINIK SCHWARZ [1] (Graduate Student Member, IEEE), STEPHAN HÄFNER [2], REINER THOMÄ [2] (Fellow, IEEE), AND CHRISTIAN WALDSCHMIDT [1] (Fellow, IEEE)

(Regular Paper)

[1]Institute of Microwave Engineering, Ulm University, 89081 Ulm, Germany
[2]Electronic Measurements and Signal Processing Group, Technische Universität Ilmenau, 98684 Ilmenau, Germany

CORRESPONDING AUTHOR: André Dürr (e-mail: andre.duerr@uni-ulm.de).

This work was supported by the Deutsche Forschungsgemeinschaft (DFG, German Research Foundation) under Project 317632307.

ABSTRACT For multistatic radar networks in the upper mm-wave range with a large spacing between its radar sensor nodes, a coherent signal distribution is very complex and thus very costly. Hence, it is desirable to generate the mm-wave signals individually for each radar sensor node, i.e., non-coherently. However, multistatic radar networks using a non-coherent signal distribution for its radar sensor nodes are affected by systematic errors and uncorrelated phase noise, which reduces the resolution and the detection performance of these systems. In this article, a novel non-coherent signal synthesis concept based on the direct digital synthesis (DDS) principle is presented for multistatic radar networks. Compared to a signal synthesis using a phase-locked loop (PLL), it is shown that the different phase noise behavior of the DDS is beneficial for bistatic signal paths between the radar sensor nodes. The presented hardware concept is considered and analyzed for three different types of coherency regarding the signal distribution: coherent, quasi-coherent, and incoherent. Measurements with a multiple-input multiple-output (MIMO) radar at 150 GHz prove that despite a non-coherent signal distribution, it is possible to achieve the same detection and imaging performance as with a fully coherent radar by using a DDS.

INDEX TERMS Bistatic radar, chirp sequence modulation, coherency, DDS, direction-of-arrival (DoA) estimation, frequency modulated continuous wave (FMCW), imaging radar, millimeter-wave radar, MIMO radar, multistatic radar, phase noise correlation, PLL, radar networks.

I. INTRODUCTION

Besides Lidar, camera, and ultrasound, imaging radar is a key sensing technology that is meanwhile frequently used in a lot of automotive [1], industrial [2], civil [3], military [4], and security applications [5]. Millimeter-wave imaging radars are able to determine the range, velocity, and DoA of a radar target but require phase coherent signals.

Typically, the mm-wave signal stems from one signal source and is distributed coherently to all hardware channels [6]–[9]. Thus, the phase noise is correlated and partly cancels within the intermediate frequency (IF) signal [10], which improves the detection performance of these radar systems. However, coherent signals lead to a high hardware effort on the printed circuit board (PCB) and limit the hardware design. Due to the high signal attenuation losses, a coherent signal distribution is only feasible for radars with moderate feed line lengths to the antennas.

The increasing demand for a higher angular resolution and a higher channel diversity makes multistatic radar networks consisting of multiple radar sensor nodes [11] or radars with a very large aperture [12] more and more popular. For these types of radar systems, an incoherent signal distribution is desirable. The major drawback of an incoherent signal distribution is the need for synchronization of frequency and

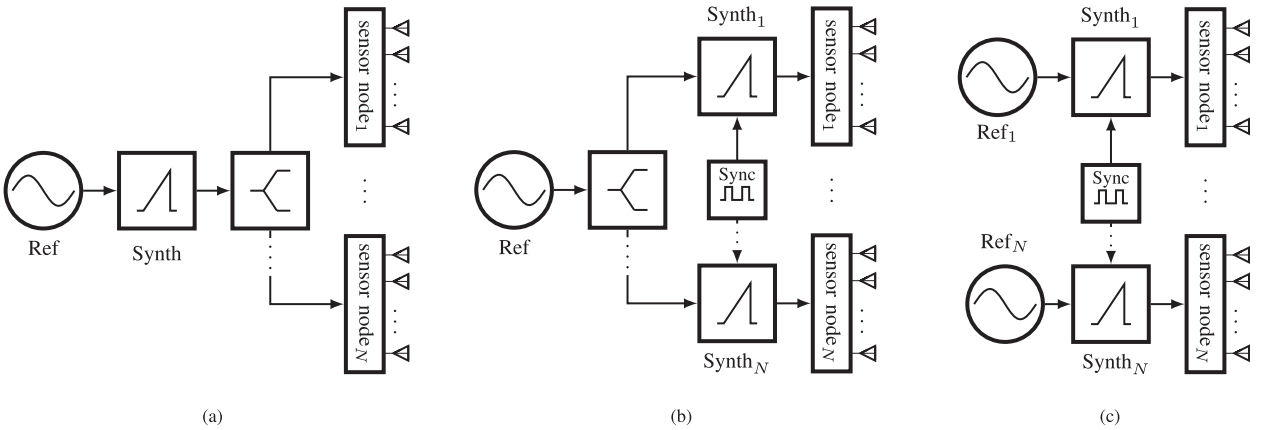

FIGURE 1. Block diagrams for different types of coherency to combine multiple sensor nodes to one MIMO system according to [13]. (a) Coherent system with one common signal synthesizer for all sensor nodes. (b) Non-coherent system with one common oscillator but individual signal synthesizers for each sensor node (quasi-coherent). (c) Incoherent system using an individual signal synthesizer and oscillator for each sensor node. The reference frequency is significantly smaller than the output frequency of the synthesizer, i.e., $f_{\mathrm{Ref}} \ll f_{\mathrm{Synth}}$.

phase in case of a coherent signal evaluation, the higher computational complexity, and the loss in detection performance due to uncorrelated phase noise [13], [14]. To exploit the full potential of signal paths between the radar sensor nodes, non-coherent hardware architectures with the same detection performance as coherent radars are needed. In the following, signal paths between the radar sensor nodes and non-coherent signal synthesis for the respective transmit (Tx) and receive (Rx) signals are called bistatic, while signal paths within a radar sensor node and coherent signal synthesis are denoted as monostatic.

The simplest way to combine different radar sensor nodes is to operate them without any synchronization and to evaluate only monostatic signal paths employing coherent signals within one radar sensor node [15]. For a large spacing between the radar sensor nodes, a target is measured from different angles, which provides additional information of the target. Since the bistatic radar responses between the radar sensor nodes are not evaluated, the full potential of the multistatic radar network cannot be exploited [16].

To evaluate the bistatic signal paths and to increase the information content about the scenery, the individual radar sensor nodes must be synchronized [11], [17]–[20]. Due to systematic errors, it is not possible to estimate the DoA without a proper error correction in signal processing. Because of uncorrelated phase noise in bistatic signal paths, the detection performance is significantly reduced, which degrades the quality of the estimated radar parameters.

As shown in [13], [14], the systematic errors can be corrected exploiting a known target in the radar channel or alternatively by means of a parasitic coupling path within the radar system. This allows the evaluation of bistatic radar responses with the same detection performance as for monostatic radar responses and to perform a DoA estimation with all monostatic and bistatic radar responses. The requirements of the signal processing can be relaxed if a common oscillator is distributed to all signal synthesizers [13], [21], [22]. However, the bistatic radar responses are still affected by uncorrelated phase noise. This can be minimized by a signal processing as shown in [14]. The main disadvantage of a subsequent phase noise cancellation in signal processing is the high computational effort and the necessity to detect a dominant target besides an increased noise level.

In this work, a novel hardware architecture for non-coherent multistatic radar networks is presented. The signal synthesizer is based on the architecture presented in [23], which uses the principle of a DDS. Compared to [23], each radar sensor node within the network is implemented with its own signal synthesizer. Therefore, bistatic signal paths between the radar sensor nodes are relevant and are also evaluated. A phase noise analysis is performed and compared to a signal synthesis using a PLL. With the proposed hardware architecture, it is possible to realize multistatic radar networks with non-coherent signal synthesis but the same detection performance as for coherent radars. The results presented in this article are a milestone in multistatic radar networks and show for the first time that the same detection performance can be achieved both for monostatic and bistatic signal paths despite non-coherent signals.

The article is organized as follows: The different types of coherency are introduced in Section II. Afterwards, the typical error sources in bistatic radar responses are summarized in Section III, and a phase noise analysis is conduced for both a signal synthesis using a DDS and a PLL. The theory is verified by radar measurements in Section IV for different types of coherency and both signal synthesis variants. Finally, the overall imaging performance of the multistatic radar network is shown for the quasi-coherent and incoherent case when using the DDS as signal synthesizer.

II. DIFFERENT TYPES OF COHERENCY

In general, imaging radars are realized with a coherent signal distribution concept as depicted in Fig. 1(a). For this purpose, a centrally generated high-frequency signal is distributed to all

Tx and Rx antennas using a signal distribution network. This ensures that the phase relations between all hardware channels are constant and only need to be calibrated once before performing a DoA estimation [24]. As the signal distribution on the PCB is lossy, the maximum feed line length is limited, which mainly depends on the distribution frequency and the used materials.

Especially for multistatic radar networks, a coherent signal distribution for the high-frequency signals is not feasible, as it is very complex and thus costly for increasingly large spacings between the radar sensor nodes. This limitation in the hardware design can be solved if the signal synthesis is realized non-coherently for each radar senor node [13].

In Fig. 1(b), a non-coherent signal distribution as in [13], [21], [22] is shown, where one common reference oscillator at a significantly lower frequency than the output frequency of the signal synthesizer ($f_{\mathrm{Ref}} \ll f_{\mathrm{Synth}}$) is shared between all synthesizers. As the generated signals are referred to a common oscillator, the requirements for the signal distribution network are reduced. In this article, this system configuration is denoted as quasi-coherent.

Alternatively, the hardware effort can be further reduced if the signal distribution is realized fully incoherently and thus, no common reference signals are shared (see Fig. 1(c)).

In both non-coherent cases (quasi-coherent and incoherent), the high-frequency signal is generated individually in each radar sensor node. The number of systematic errors as well as the achievable detection performance differ for the different types of coherency and for the different signal synthesizer architectures. In the following, these errors and the expected phase noise correlation is derived and compared for both signal synthesizer concepts (PLL and DDS) and the quasi-coherent and incoherent system setup.

III. ERROR AND PHASE NOISE ANALYSIS

In this section, the errors in bistatic signal paths are outlined, and a phase noise model is derived when using the DDS and the PLL as signal synthesizer in non-coherent radars. Finally, the derived theory is verified by measurements.

A. ERROR SOURCES IN NON-COHERENT RADARS

The used signal distribution and system concept directly determine the systematic errors. Since different signal synthesizers (quasi-coherent system, Fig. 1(b)) and even reference oscillators (incoherent system, Fig. 1(c)) are used, the signals are not phase-locked at the operating frequency as in the coherent system in Fig. 1(a). The occurring errors are extensively described in [13], [14] and are therefore only briefly summarized here.

Due to the different oscillators in the incoherent system (see Fig. 1(c)), the bistatic radar response is affected by the following errors: A start time and frequency error causes a range offset, a ramp slope error leads to a change of the evaluated range within the ramp duration, a start phase difference between the signal synthesizers affects the DoA estimation capability, and uncorrelated phase noise influences the noise level and the detection performance. When using one common reference oscillator, only the start phase difference and partially uncorrelated phase noise remain, as all other errors are caused by the slightly different oscillation frequencies of the oscillators. These errors can be corrected in signal processing using a known static target [13] or with one dominant target in the radar channel [14].

B. FREQUENCY SYNTHESIS WITH PLL

The simplified block diagram of a typical PLL circuit is shown in Fig. 2(a). The closed loop consists of a reference oscillator with low phase noise (Ref), a phase-frequency detector (PFD), a charge pump (CP), a frequency divider with factor K, a low-pass filter (LF), and a voltage-controlled oscillator (VCO). In order to generate FMCW signals either the reference source can be modulated, or a variable frequency divider can be used. The synthesizer in this work was exemplarily realized using the device LMX2492 from Texas Instruments in combination with the wideband VCO HMC6380 from Hittite. The advantage of the signal synthesis using a PLL is the high spectral purity and its low power consumption (LMX2492: 0.2 W, HMC6380: 0.38 W). The theoretical principles of PLLs are extensively studied in [25]–[28].

In the following, the phase noise sources of the output signal of a PLL are summarized. Phase noise is described by its power spectral density $\mathcal{L}_{\Phi}$. Since the individual sources are assumed as uncorrelated, the phase noise $\mathcal{L}_{\Phi,\mathrm{PLL,Out}}$ at the output of a PLL is given by an additive superposition of the phase noise contributions $\mathcal{L}_{\Phi}$ from the individual PLL components [29]:

$$\mathcal{L}_{\Phi,\mathrm{PLL,Out}}(f) = \mathcal{L}_{\Phi,\mathrm{Ref}}(f) + \mathcal{L}_{\Phi,\mathrm{PFD}}(f) + \mathcal{L}_{\Phi,\mathrm{LF}}(f) + \mathcal{L}_{\Phi,\mathrm{VCO}}(f). \quad (1)$$

The output phase noise of the PLL is influenced by the phase noise source of the reference oscillator ($\mathcal{L}_{\Phi,\mathrm{Ref}}$), the PFD ($\mathcal{L}_{\Phi,\mathrm{PFD}}$), the LF ($\mathcal{L}_{\Phi,\mathrm{LF}}$) and the VCO ($\mathcal{L}_{\Phi,\mathrm{VCO}}$). The corresponding transfer functions to the output in (1) are already included within the individual phase noise contributions [26]. Thus, the output phase noise of a PLL can only be improved by considering all phase noise sources and reducing the dominant part of the output phase noise.

C. FREQUENCY SYNTHESIS WITH DDS

The signal synthesis using a DDS is performed by digital samples. One possible realization of a high-frequency signal synthesis using a DDS is shown in Fig. 2(b). The DDS circuit consists of a reference oscillator (Ref), an optional frequency divider with factor K, a phase accumulator, a phase-to-amplitude converter (PAC), and a digital-to-analog converter (DAC). The synthesizer in this work was exemplarily realized using the device AD9914 from Analog Devices.

In contrast to the PLL, the reference frequency of the oscillator must be at least twice as large as the highest generated frequency to satisfy the sampling theorem. Thus, the DDS clock is significantly higher in comparison to the PLL clock.

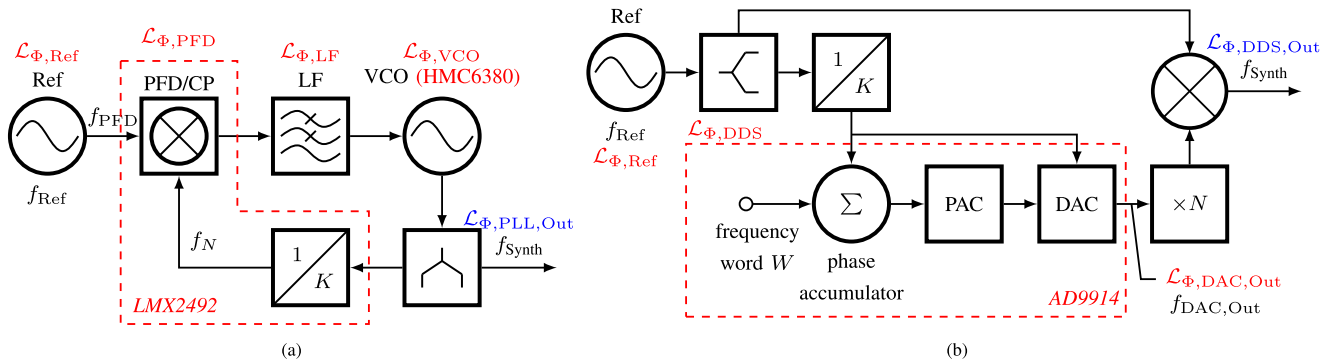

FIGURE 2. **Block diagrams of two typical circuits to synthesize mm-wave signals. The individual phase noise sources are marked in red. (a) PLL. (b) DDS including a multiplier by factor *N*, and a mixer to increase the output frequency.**

To generate even higher frequencies, the DDS output signal must be translated to the desired frequency band. This can be done by a frequency multiplication, an up-conversion with a mixer, or a combination of both as shown in Fig. 2(b). Alternatively, it is possible to use higher Nyquist bands, or the DDS can be used to generate a low-frequency FMCW signal, which is then stabilized with a PLL and an integer divider in the control-loop [30]. The advantage of the DDS is its high frequency resolution. Disadvantages are the high power consumption of the DAC (AD9914: 2.4 W) and the poorer spectral purity (primary phase truncation spurs, harmonics, images of higher Nyquist bands) compared to the PLL, which requires one or multiple complex filtering stages [31].

The phase noise $\mathcal{L}_{\Phi,\mathrm{DAC,Out}}$ at the output of the DAC consists of the sum of the phase noise of the reference oscillator $\mathcal{L}_{\Phi,\mathrm{Ref}}$ and the internal phase noise $\mathcal{L}_{\Phi,\mathrm{DDS}}$ of the DDS circuit and is given by [32]

$$\mathcal{L}_{\Phi,\mathrm{DAC,Out}}(f)=\left(\frac{f_{\mathrm{DAC,Out}}}{f_{\mathrm{Ref}}}\right)^2\mathcal{L}_{\Phi,\mathrm{Ref}}(f)+\mathcal{L}_{\Phi,\mathrm{DDS}}(f). \quad (2)$$

The internal phase noise of the DDS circuit includes the flicker noise and the thermal noise of the DAC. It has to be noted that the frequency divisor with factor K is already included in the ratio of the frequencies. The output phase noise can be improved using a reference oscillator with lower phase noise as long as the phase noise of the reference is better than the phase noise source of the circuit. In case that the frequency conversion is realized using a mixer with correlated signals coming from a single signal source and a frequency multiplier (see Fig. 2(b)), the phase noise at the output of the DDS results in [33]

$$\mathcal{L}_{\Phi,\mathrm{DDS,Out}}(f) = \left(N\frac{f_{\mathrm{DAC,Out}}}{f_{\mathrm{Ref}}}+1\right)^2\mathcal{L}_{\Phi,\mathrm{Ref}}(f) + N^2\mathcal{L}_{\Phi,\mathrm{DDS}}(f). \quad (3)$$

D. PHASE NOISE CORRELATION FOR DIFFERENT TYPES OF COHERENCY

The essential quantity to describe the signal quality and the detection performance within a radar measurement is the signal-to-noise ratio (SNR). The received signal power is given by the radar equation and depends on the transmitted power, the antenna gain, the free-space loss, and the radar cross section of the target [34]. In contrast, the noise power is composed of several sources along the signal path and is a superposition of thermal noise, quantization noise, and phase noise [35]. Typically, analog-to-digital converters (ADCs) within the radar monolithic microwave integrated circuit (MMIC) have 12 or more effective bits [8], which means that the quantization noise level is much smaller than the thermal noise level and can therefore be neglected. The thermal noise level is given by the receive chain and is thus identical for monostatic and bistatic radar responses. The phase noise power directly depends on the system concept and differs significantly for monostatic and bistatic radar responses and the types of coherency. In the following, the influence on the phase noise is analyzed for both synthesizer architecture (DDS and PLL) and for the different types of coherency.

1) COHERENT SYSTEM

For the coherent system (see Fig. 1(a)), the Tx and Rx signals stem from the same signal synthesizer. Thus, the phase noise of the signals is correlated, and the range correlation effect occurs [10]. The phase noise $\mathcal{L}_\Phi$ within the IF signal cancels depending on the time delay τ of the signal in the radar channel and the frequency offset f from the carrier. The range correlation effect is valid for both synthesizer architectures, and the residual phase noise $\mathcal{L}_{\Delta\Phi}$ after the output of the receive mixer is given by

$$\mathcal{L}_{\Delta\Phi}(f) = \mathcal{L}_\Phi(f)\left[2-2\cos(2\pi f\tau)\right]. \quad (4)$$

The term within the brackets of (4) describes the phase noise cancellation factor due to the range correlation effect. It is valid for both continuous wave Doppler radars and homodyne FMCW radars [35].

2) QUASI-COHERENT SYSTEM

If a common reference oscillator is used as in the quasi-coherent system (see Fig. 1(b)), the range correlation effect according to (4) has only an impact on the phase noise source

of the reference oscillator. In this case, the phase noise at the output of the receive mixer is partly correlated [7]. All other phase noise sources superimpose and lead to an increase of the initial phase noise by 3 dB in case of two identical synthesizers. Based on the phase noise model given by (1) and (3), the phase noise at the output of the receive mixer is given by

$$\mathcal{L}_{\Delta\Phi,\mathrm{PLL,q-coh}}(f) = \left[2 - 2\cos(2\pi f\tau)\right]\mathcal{L}_{\Phi,\mathrm{Ref}}(f) + 2\left(\mathcal{L}_{\Phi,\mathrm{PFD}}(f) + \mathcal{L}_{\Phi,\mathrm{LF}}(f) + \mathcal{L}_{\Phi,\mathrm{VCO}}(f)\right) \quad (5)$$

$$\mathcal{L}_{\Delta\Phi,\mathrm{DDS,q-coh}}(f) = 2N^2\mathcal{L}_{\Phi,\mathrm{DDS}}(f) + \left[2 - 2\cos(2\pi f\tau)\right] \cdot \left(N\frac{f_{\mathrm{DAC,Out}}}{f_{\mathrm{Ref}}} + 1\right)^2 \mathcal{L}_{\Phi,\mathrm{Ref}}(f). \quad (6)$$

Compared to the DDS, the output phase noise of the PLL is not only influenced by the phase noise source of the PFD ($\mathcal{L}_{\Phi,\mathrm{PFD}}$) and reference oscillator ($\mathcal{L}_{\Phi,\mathrm{Ref}}$) but also by the phase noise of the LF ($\mathcal{L}_{\Phi,\mathrm{LF}}$) and the VCO ($\mathcal{L}_{\Phi,\mathrm{VCO}}$). Typically, the output phase noise of a PLL is dominated by the reference oscillator for small frequency offsets from the carrier. For these small frequency offsets, a quasi-coherent system can improve the output phase noise. Also, if a low quality reference oscillator raises the overall output phase noise of the PLL, a quasi-coherent system is beneficial, too.

On the other hand, the phase noise of the DDS is only determined by the phase noise of the circuit and the reference oscillator. By canceling the phase noise of the reference oscillator (see (6)), the internal phase noise has a major influence on the residual phase within the IF signal. Hence, the output phase noise of the DDS is only marginally influenced by the phase noise of the reference oscillator and is mainly given by the internal phase noise of the circuit. It has to be mentioned that the internal phase noise is mainly produced by the finite resolution of the DAC and typically lower compared to a PLL [36].

3) INCOHERENT SYSTEM

Due to the two completely independent signal synthesizers, the noise processes at the receiver output are completely uncorrelated for bistatic radar responses. Thus, the phase noise at the receiver output can be calculated as an additive superposition of the phase noise sources of the two signal synthesizers involved in the IF signal:

$$\mathcal{L}_{\Phi,\mathrm{incoh}}(f) = \mathcal{L}_{\Phi,\mathrm{Synth}_1}(f) + \mathcal{L}_{\Phi,\mathrm{Synth}_2}(f). \quad (7)$$

Therefore, the resulting phase noise in the IF signal can only be reduced by improving the output phase noise of the individual signal synthesizers.

E. PROOF OF THE PHASE NOISE CANCELLATION

The phase noise model and the expected partial phase noise correlation for the quasi-coherent system realization is evaluated experimentally with the measurement setup shown in Fig. 3. To measure the phase noise by means of a signal source analyzer, the signal of one signal synthesizer is shifted by the frequency f_{XCO} using a low-frequency crystal oscillator (XCO) [7]. To ensure that the XCO has no influence on the phase noise of the signal synthesis, the XCO must have significantly smaller phase noise than the generated signal at the output of the signal synthesizer, i. e., $\mathcal{L}_{\Phi,\mathrm{XCO}} \ll \mathcal{L}_{\Phi,\mathrm{Synth}}$. The residual phase noise $\mathcal{L}_{\Delta\Phi}$ at the output of the mixer can be measured with a signal source analyzer at the frequency f_{XCO}. In order to verify the phase noise correlation, the phase noise level is adjusted for both signal synthesizer variants (PLL and DDS) using reference oscillators of different quality. In case of the DDS, the input frequency of 2.5 GHz is firstly derived from a high quality dielectric resonator oscillator (DRO) at 10 GHz. In the second case, the 10 GHz signal is generated with a PLL with a significantly inferior phase noise performance. Compared to the DDS, the input frequency of the PLL is significantly lower due to the different operating principle. In the first case, the reference oscillator is a high quality XCO$^+$ at 100 MHz with very low phase noise and in the second case a low quality oscillator XCO$^-$ at 100 MHz with poor phase noise performance. The system realizations are summarized in Table 1. Since the transmission line lengths to the mixer are identical, and the group delay of the mixer is negligibly small, the signal delay τ is almost zero, and the correlation of the phase noise of the reference oscillator is maximum. Thus, the measurements show the best achievable system performance.

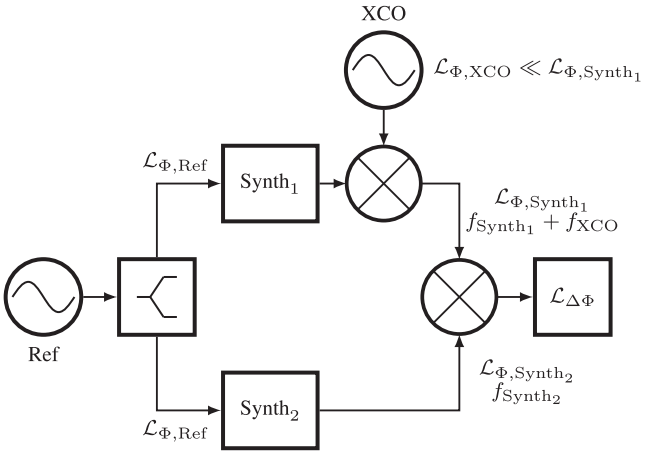

FIGURE 3. Simplified block diagram of the measurement setup as in [7] to verify partially correlated phase noise in the quasi-coherent setup.

TABLE 1. Overview of the Different System Realizations

quasi-coh.	**DDS** with Ref	① DRO	② PLL
	PLL with Ref	③ XCO$^+$	④ XCO$^-$
incoherent	**DDS** with Ref	⑤ 2 × DRO	⑥ 2 × PLL
	PLL with Ref	⑦ 2 × XCO$^+$	⑧ 2 × XCO$^-$
	$\mathcal{L}_{\Phi,\mathrm{Ref}}$	high quality	low quality

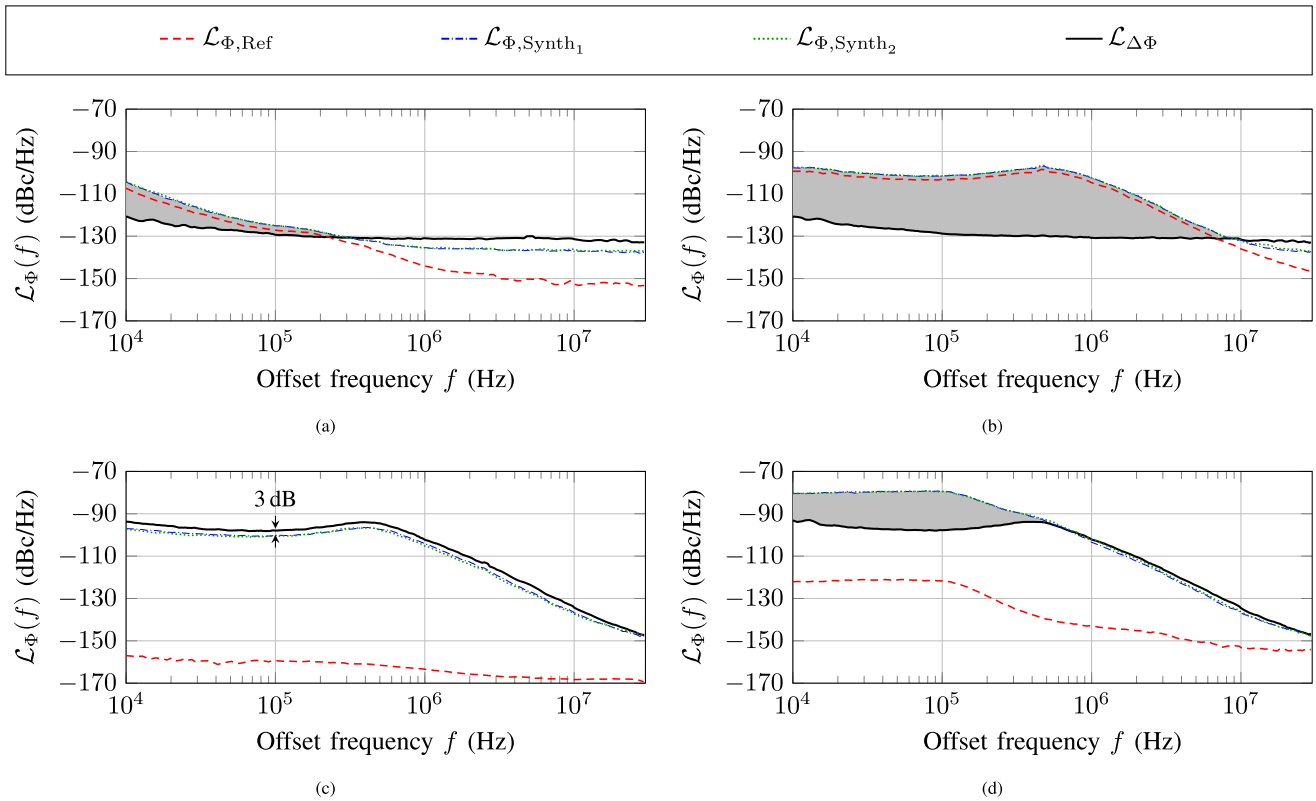

FIGURE 4. **Measured phase noise and resulting phase noise cancellation (marked as gray area) for the quasi-coherent system setup with the system configurations according to Table 1. (a) DDS with DRO (10 GHz, high quality) ①. (b) DDS with PLL (10 GHz, low quality) ②. (c) PLL with XCO (100 MHz, high quality) ③. (d) PLL with XCO (100 MHz, low quality) ④.**

The phase noise measurements and the resulting phase noise cancellation for both signal synthesizer variants (DDS and PLL) and different phase noise levels of the reference oscillator are compared in Fig. 4. According to Section III-III-C and (3), the output phase noise $\mathcal{L}_{\Phi,\mathrm{Synth}_{\{1,2\}}}$ of the DDS is given by the superposition of the phase noise of the reference oscillator $\mathcal{L}_{\Phi,\mathrm{Ref}}$ scaled to the output frequency (cf. (3)) and the internal phase noise $\mathcal{L}_{\Phi,\mathrm{DDS}}$ of the circuit, which is proven by the composition of the curve shape of $\mathcal{L}_{\Phi,\mathrm{Synth}_{1,2}}$ (see Fig. 4(a) and (b)). The residual phase noise $\mathcal{L}_{\Delta\Phi}$ (—) at the receiver output is the same for both reference phase noise levels and shows the range correlation of the phase noise of the reference oscillator (see the gray marked area). In both cases, the mixer output corresponds to the internal phase noise $\mathcal{L}_{\Phi,\mathrm{DDS}}$ of the DDS circuit and is determined by flicker noise ($\propto 1/f$) for small frequency offsets and thermal noise for larger frequency offsets from the carrier.

For the PLL, the following relationships apply: If a high quality oscillator with low phase noise is used (see Fig. 4(c)), the output phase noise of the PLL is not influenced by the reference oscillator. Thus, the phase noise at the output of the receive mixer (—) is the additive superposition of the phase noise of both PLLs, leading to an increase of the phase noise level of 3 dB and shows that no improvement due to a range correlation occurs. If a low quality reference oscillator is used and the output phase noise of the PLL is thus raised by the oscillator, the range correlation leads to an improvement of the phase noise at the receiver output (see Fig. 4(d)).

This implies that for the quasi-coherent system a reference of lower quality can be used to achieve the same system behavior as with a high quality reference. Since the range correlation effect reduces for larger signal delays, it is necessary to take the maximum expected signal delay into account while determining the needed quality of the reference.

Based on the range correlation measurements of the quasi-coherent system in Fig. 4, a performance evaluation can also be provided for the incoherent system. According to (7), the incoherent system operation leads to an increasing residual phase noise by 3 dB. This means that with the incoherent system a deterioration in detection performance in comparison to the quasi-coherent system occurs if the reference oscillator is worse than the residual phase noise. This is the case in Fig. 4(a) for small frequency offsets up to approximately 200 kHz and in Fig. 4(b) for offset frequencies up to 10 MHz, where the phase noise level of the reference oscillator (PLL) is about 25 dB above the internal phase noise of the DDS.

For the PLL realization using a high-quality XCO (see Fig. 4(c)), no difference in the detection performance between quasi-coherent and incoherent signal couplings can be expected, because the reference oscillator does not influence the

output phase noise of the PLL. Using a reference oscillator of low quality (see Fig. 4(d)), the output phase noise of the synthesizer is raised up to an offset frequency of approximately 400 kHz. For the incoherent system this deteriorates the detection performance of up to 20 dB (gray area) in contrast to the quasi-coherent system.

IV. VERIFICATION BY RADAR MEASUREMENTS

The theoretical derivations from Section III, which were shown using continuous wave measurements, are applied and verified in the following sections based on the achievable detection performance and the overall imaging performance for the quasi-coherent and incoherent operation mode (see Fig. 1(b) and (c)) in FMCW radar measurements.

A. HARDWARE DEMONSTRATOR

The radar demonstrator used for the verification of the theory is depicted in Fig. 5. The radar is composed of two radar sensor nodes, each with eight single-channel radar MMICs and integrated on-chip antennas for both the Tx and Rx signal paths [37]. The block diagram of the FMCW MIMO radar is shown in Fig. 5(a) and the used architecture of the MMIC in (b). The radar parameters used for the measurements are summarized in (c). The radar bandwidth of $B = 7.2\,\text{GHz}$ results in a range resolution of $\delta R \approx 2.1\,\text{cm}$. A photograph of the multistatic radar network with an overall virtual aperture size of 196.5 λ is depicted in Fig. 5(d). Additionally, a photograph and a schematic illustration of the measurement hardware are given in Fig. 5(e) and (f).

The thermal noise level P_{th} can be calculated by [35]

$$P_{\text{th}} = k_{\text{B}} T_{\text{n}} B_{\text{n}} G_{\text{Rx}} = k_{\text{B}} (F_{\text{n}} - 1) \frac{T_0}{T_c} G_{\text{Rx}} = -67\text{dBm}\,, \qquad (8)$$

with the equivalent noise temperature T_{n}, the temperature $T_0 = 290\text{K}$, the noise figure $F_{\text{n}} = 16$ dB, the Boltzmann constant k_{B}, the receiver gain $G_{\text{Rx}} = 51$ dB, and the noise bandwidth $B_{\text{n}} = 1/T_c = 1/100\,\mu\text{s}$.

B. DETECTION PERFORMANCE

This section deals with the detection performance in terms of the expected SNR is evaluated for a bistatic radar response for all types of coherency (see Fig. 1) and both signal synthesizer variants (DDS and PLL, see Fig. 2) in comparison. The overall noise level of a single measurement P_{N} is determined by calculating the standard deviation over $N_c = 32$ ramps [7]. The theoretical noise level is simulated based on the results from Section III using (5) and (6) and compared to the measured noise level.

1) COHERENT SYSTEM

An evaluation of the detection performance for coherent, highly integrated short-range radars in the upper millimeter-wave range was already conducted in [37], [38]. It was shown that fully coherent short-range radars are typically thermally noise limited due to the high range correlation factor, see (4). An exemplary noise budget of the coherent system is given in Table 2 for typical values at a frequency offset $f = 350\,\text{kHz}$ and a signal delay $\tau = 23.5\,\text{ns}$ (corresponds to the beat frequency $f_b = 1.7\,\text{MHz}$ or the range $R = 3.5\,\text{m}$). The phase noise is measured at the synthesizer output frequency $f_{\text{Synth}} = 12.85\,\text{GHz}$ and converted to the center frequency $f_{\text{c}} = 154.2\,\text{GHz}$. The noise estimation reveals that the noise level due to phase noise P_{PN} is 14,5 dB below the thermal noise level. Thus, this radar system is thermally noise limited.

TABLE 2. Exemplary Noise Estimation in the Coherent System

parameter	value
receive power*	−21 dBm
phase noise*,+ ($f_{\text{c}} = 154.2\,\text{GHz}$, $f = 350\,\text{kHz}$)	−74.75 dBc/Hz
noise bandwidth+ ($T_r = 100\,\mu\text{s}$)	40 dB Hz
range correlation factor+ ($\tau = 23.5\,\text{ns}$, (4))	−25.75 dB
noise level due to phase noise+	−81.5 dBm
thermal noise level+	−67 dBm

* measured + calculated

This noise estimation can be calculated for each frequency offset from the carrier and thus for all beat frequencies. It shows that the detection performance is always determined by the thermal noise level.

2) QUASI-COHERENT SYSTEM

Due to the usage of a common reference oscillator, the cancellation factor from (4) only affects the phase noise of the reference oscillator, see (5) and (6).

According to (6), the phase noise of the DDS is determined by the phase noise of the reference oscillator and the internal phase noise of the DDS circuit. Thus, an improvement of the residual phase noise at the receiver output is achieved if the phase noise of the reference oscillator is worse than that of the DDS circuit and improves due to the phase noise cancellation factor regarding the phase noise of the reference oscillator. Hence, the internal phase noise of the DDS circuit is expected to dominate the radar measurement in the quasi-coherent system.

These theoretical results from Section III are verified and compared in Fig. 6(a) and (b) by means of radar measurements using the DDS and reference oscillators of different quality. Due to the constant curve shape of the measured noise level (- - -) and the agreement with the theoretically derived thermal noise level (-·-·-), it follows that the measurements with the DDS are thermally noise limited in both cases despite different output phase noises of the signal synthesizers. Thus, there is no difference in the detection performance if compared to the coherent system [37]. At an exemplary frequency offset of $f = 350\,\text{kHz}$, the simulated phase noise power for the DDS with DRO (see Fig. 6(a)) is about 20,5 dB below the thermal noise level. According to the theory, it is only determined by the internal phase noise of the DDS circuit. When using a low quality reference oscillator (DDS with PLL), the simulated

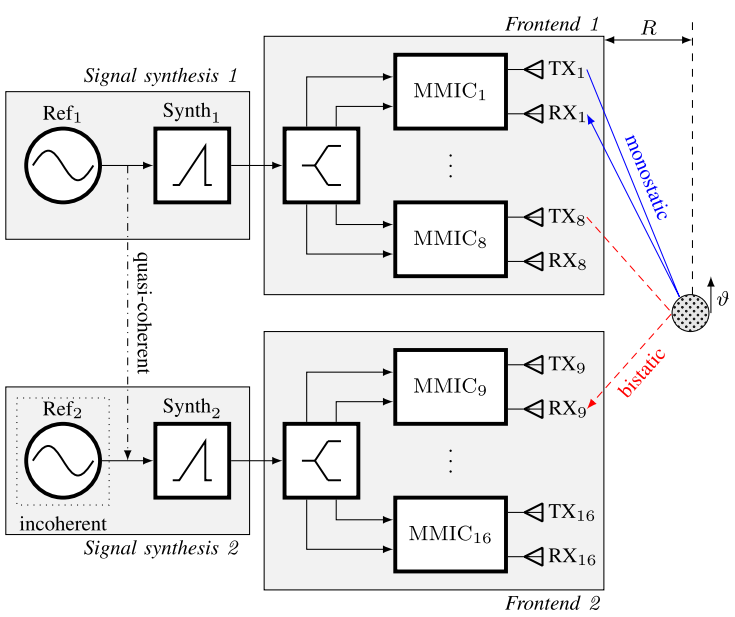

(a)

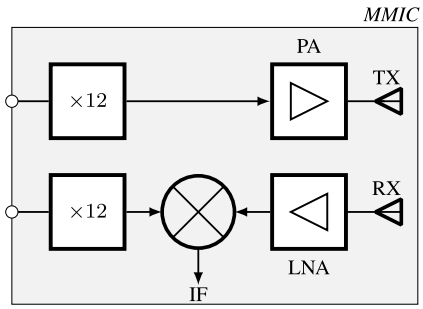

(b)

description	symbol	value
output frequency (synth.)	f_{Synth}	$12.5 - 13.1\,\mathrm{GHz}$
radar center frequency	f_c	$154.2\,\mathrm{GHz}$
radar bandwidth	B	$7.2\,\mathrm{GHz}$
ramp duration (pause)	T_c (T_r)	$100\,\mu\mathrm{s}$ ($250\,\mu\mathrm{s}$)
# ramps / channel	N_c	32
receiver gain	G_{Rx}	$51\,\mathrm{dB}$
total noise figure	F_n	$16\,\mathrm{dB}$

(c)

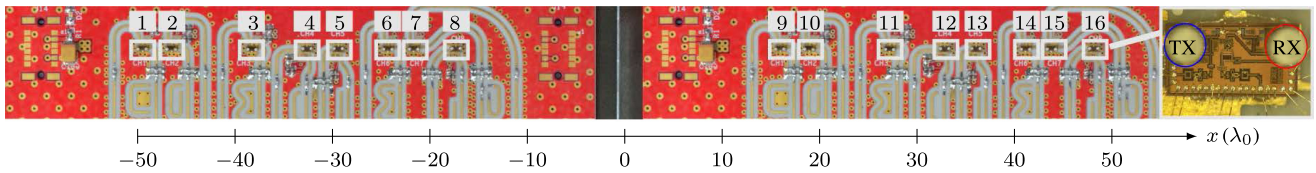

(d)

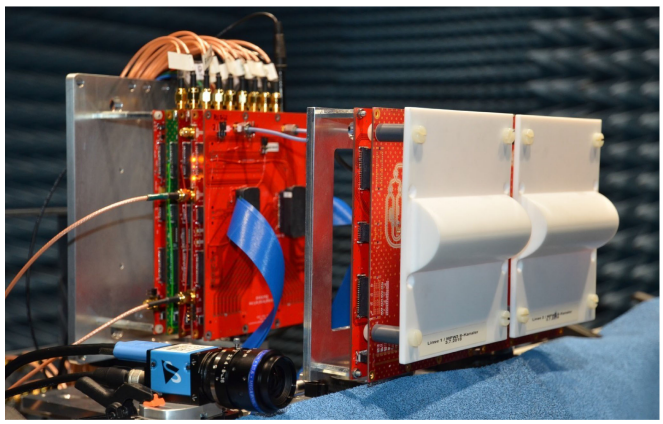

(e)

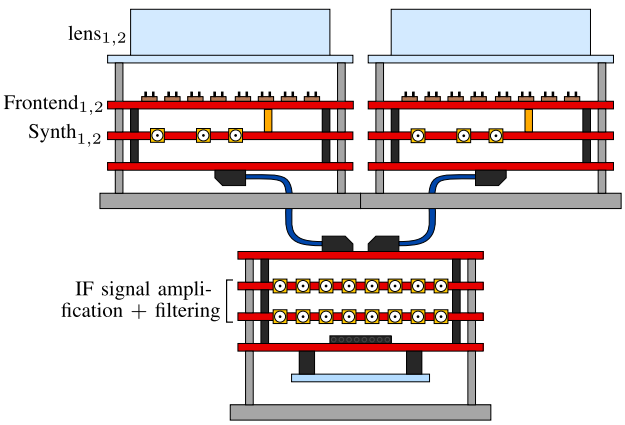

(f)

FIGURE 5. **(a) Block diagram of the radar system and measurement setup used for the measurement verification. (b) Architecture of the MMIC. (c) Radar parameters used for the verification. (d) Photograph of the antenna frontend consisting of two two radar sensor nodes, each equipped with 8 radar MMICs. (e) Photograph and (f) schematic illustration of the measurement hardware.**

phase noise power increases by 8,7 dB (–87,5 dBm → –78,8 dBm) as it is also affected by the phase noise of the oscillator in addition to the internal phase noise of the DDS circuit.

In comparison, the output phase noise of the PLL is also influenced by the VCO and the LF. An improvement due to correlated phase noise can only be achieved if the output phase noise is raised by a low quality reference oscillator. Using the PLL (see Fig. 6(c) and (d)) a loss in detection performance due to uncorrelated phase noise has to be expected. The measured noise level is in good agreement with the simulated phase noise level (·····). For a receive power of –22,5 dBm, the noise level increases by 15,5 dB compared to the thermal noise level. The difference in simulated phase noise power of about 27 dB between DDS with the PLL as reference oscillator and the PLL corresponds to the non-existent cancellation factor in (5) on the LF, the VCO, and the internal phase noise of the PLL circuit. Furthermore, the receive power differs by about 1 dB.

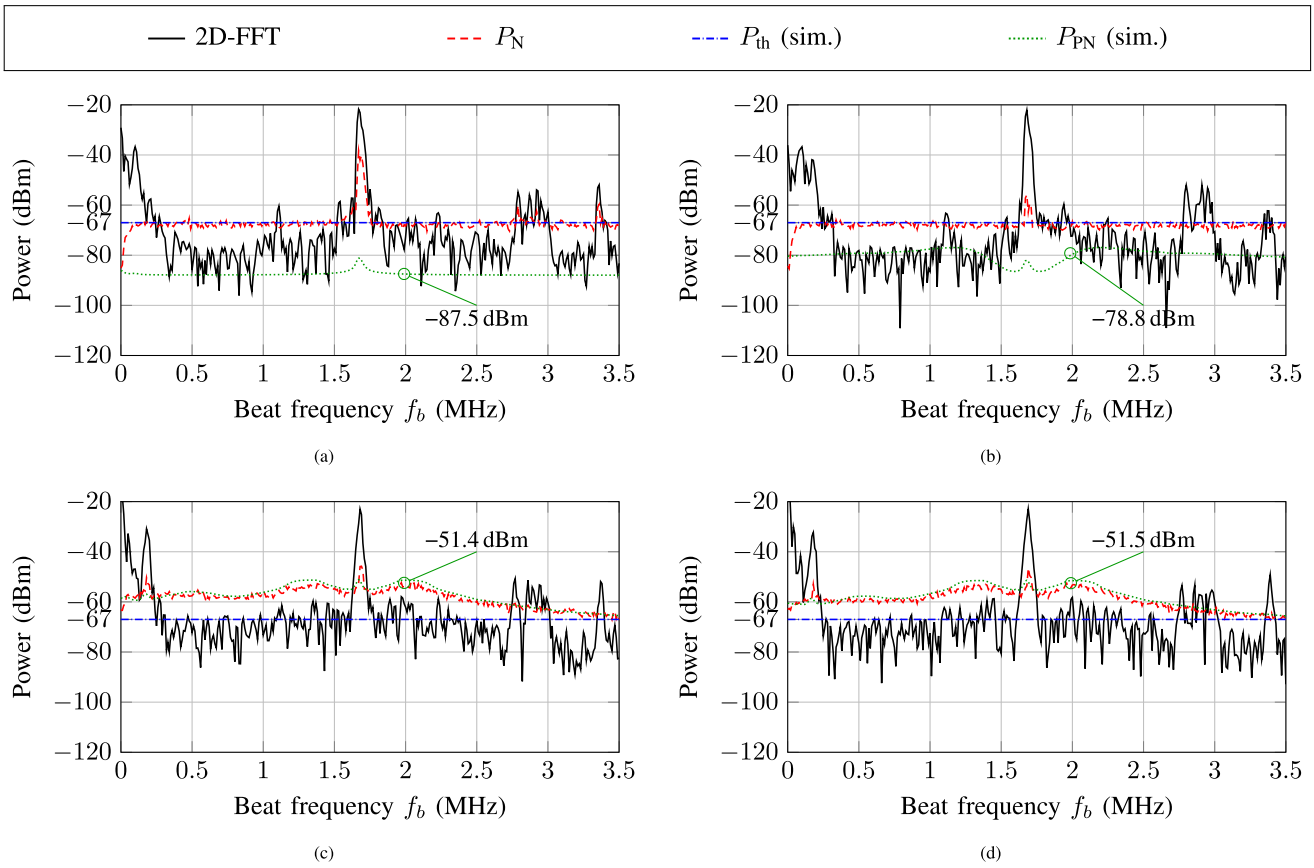

FIGURE 6. Measured detection performance of the quasi-coherent system. (a) DDS with DRO (10 GHz, high quality) ①. (b) DDS with PLL (10 GHz, low quality) ②. (c) PLL with XCO (100 MHz, high quality) ③. (d) PLL with XCO (100 MHz, low quality) ④.

The measurements prove that using a DDS the same detection performance can be achieved with reference oscillators of different quality, because the range correlation suppresses the phase noise source of the reference oscillator. This advantage cannot be fully exploited with the PLL as the phase noise sources of the VCOs, LFs, and the PLLs are always uncorrelated and dominate.

3) INCOHERENT SYSTEM

By using independent signal synthesizers, the noise processes at the receiver output are uncorrelated for bistatic signal paths. Consequently, the detection performance in radar measurements with incoherent signal generation only depends on the receive power, the output phase noise of the signal synthesizer, and the noise bandwidth. Thus, the detection performance in radar measurements can only be improved by lowering the output phase noise of the signal synthesizer.

The achievable detection performance in incoherent radar measurements is shown in Fig. 7 for both signal synthesizer variants (DDS and PLL) and for reference oscillators of different quality. The measurement from Fig. 7(a) illustrates that for the DDS with DRO the noise level is still determined by thermal noise due to the very low internal phase noise of the DDS circuit and the high quality reference oscillator. At the exemplary frequency offset $f = 350$ kHz, the simulated phase noise power is about 21 dB below the thermal noise level and is thus comparable to the quasi-coherent system. Based on the phase noise simulated according to (7), it is obvious that the phase noise power is increased for very small frequency offsets from the carrier compared to the quasi-coherent case since the reference oscillators are not correlated. This influence in the vicinity of the carrier is eliminated because of the sufficiently large distance between the receive power and the noise level due to phase noise and is thus not visible in the radar response. For larger frequency offsets, the internal phase noise of the DDS circuit is dominant. The very low internal phase noise does not influence the radar response, and there is no difference to the quasi-coherent case.

For the DDS with PLL as reference (see Fig. 7(b)), the detection performance is reduced in comparison to the quasi-coherent system (see Fig. 6(b)) due to the non-existent correlation of the reference oscillator. For a receive power of –23 dBm the noise level increases by 15,5 dB in comparison to the thermal noise level and is comparable to the PLL in the quasi-coherent system for both realizations (see Figs. 6(c) and (d)) and the PLL with reference oscillator of high quality in

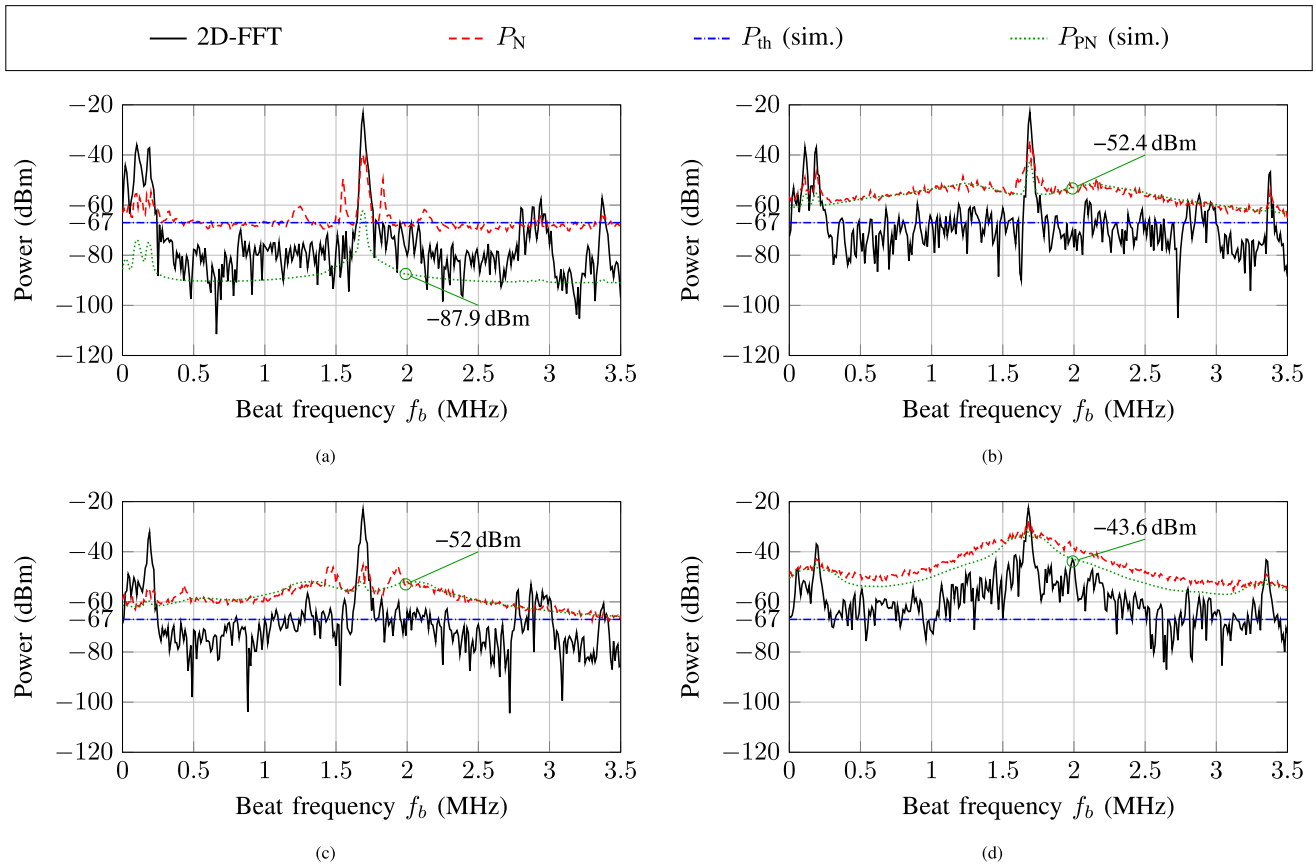

FIGURE 7. Measured detection performance of the incoherent system. (a) DDS with DRO (10 GHz, high quality) ①. (b) DDS with PLL (10 GHz, low quality) ②. (c) PLL with XCO (100 MHz, high quality) ③. (d) PLL with XCO (100 MHz, low quality) ④.

the incoherent operation mode (see Fig. 7(c)). Consequently, the internal phase noise of the PLL, the VCO, and the LF dominates the phase noise behavior.

If the phase noise of the reference oscillator is degraded in contrast to the quasi-coherent operation (see Fig. 7(d)), the detection performance is also reduced due to the non-existent correlation of the reference oscillator.

C. OVERALL IMAGING PERFORMANCE

The results from Section IV-IV-B prove that with the DDS comparable SNRs can be achieved for the coherent, quasi-coherent, and incoherent setup by minimizing all phase noise sources. In order to evaluate the influence of the different types of coherency and the related systematic errors on the imaging quality, the overall imaging performance of the multistatic MIMO radar network with DDS signal synthesizer is investigated for the measurement setup given in Fig. 5(a). The evaluation metrics are the estimation variance of range and phase, the SNR after a non-coherent integration across all channels, and the DoA estimation performance. In order to evaluate the measurement results, the received power levels of a single target in the radar channel are depicted in Fig. 8 among all channels for the quasi-coherent (see (a)) and incoherent (see (b)) case. The coherent case is included in the monostatic radar responses. Additionally, the received power level of the reference target that is used to correct all systematic errors in the incoherent case and the start phase difference between successive measurements in the quasi-coherent case is shown in Fig. 8(c). Due to the large aperture size and the violation of the far-field condition, the bistatic angle increases for antennas further apart from the array center. As a result of the angle-dependent directivity of the corner reflector and the radiation pattern of the antennas, the received power level decreases for these antennas [12]. In comparison to the radar target for monostatic radar responses, the received power of the reference target is about 25 dB lower but quite similar among the channels. In addition, the received power of the reference target is comparable to that of the main target in the outer bistatic channels.

1) ESTIMATION VARIANCE

The DoA and range estimation variances depend on an accurate estimate of the target information within the radar response. The evaluation is performed using a discrete Fourier transform (DFT) for each ramp within the ramp block. The heatmaps of the range and phase estimation variances are shown by means of its standard deviation σ for the quasi-coherent and incoherent case in comparison (see Fig. 9).

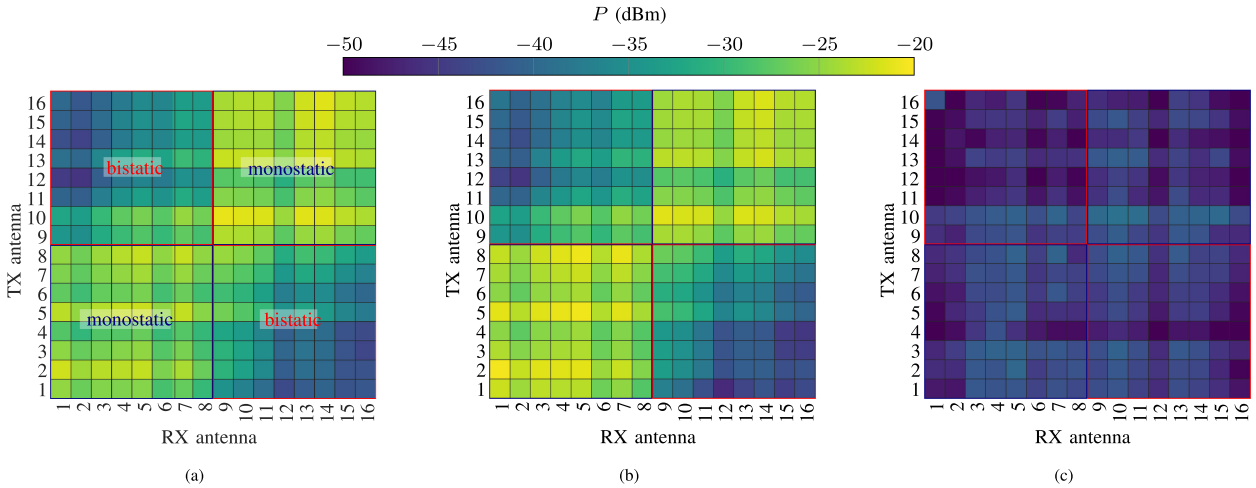

FIGURE 8. Received signal powers for all hardware channels. (a) exemplary radar target (quasi-coherent). (b) Exemplary radar target (incoherent). (c) Reference target (incoherent). In all cases, the DDS is used as signal synthesizer.

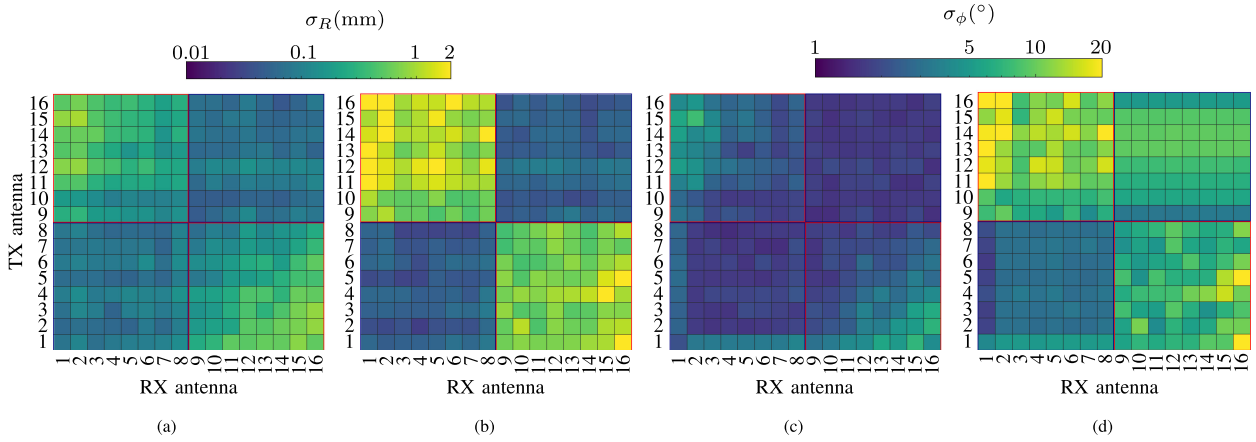

FIGURE 9. Range and phase estimation variance. (a) Range variance (quasi-coherent). (b) Range variance (incoherent). (c) Phase variance (quasi-coherent). (d) Phase variance (incoherent).

The coherent case is included within the monostatic radar responses.

The results show that the same trend yields for the range and phase estimation. However, the results differ between the incoherent and the quasi-coherent setup. For the quasi-coherent cases (Figs. 9(a) and (c)) the estimation variance depends on the receive power and the resulting SNR (cf. Fig. 8(a)). Hence, the standard deviation increases with a lower SNR. Furthermore, there is no clear difference between monostatic and bistatic radar responses.

For the incoherent case, there is a distinct difference between monostatic and bistatic radar responses. Whereas the estimation variance for monostatic radar responses is comparable to the quasi-coherent case, the estimation variance is significantly worsened for bistatic radar responses. This distinction arises due to systematic errors caused by the different oscillators, which have to be corrected. In the measurements, this error correction is conducted by means of the reference target [13]. As the SNR of the reference target is comparable in all channels and significantly lower than for the radar target in monostatic radar responses (see Fig. 8(c)), the quality of the error correction is low and leads to a high estimation variance in all bistatic radar responses. Hence, the estimation variance in the incoherent setup depends on the weaker of the two targets (main target or reference target). The received power of the main target in the outer bistatic channels (e.g. $\mathrm{Tx}_1\mathrm{Rx}_{16}$) is comparable to the received power of the reference target. Thus, the estimation variance in the incoherent setup is similar to that of the quasi-coherent setup for these outer bistatic channels.

2) RANGE-VELOCITY-DIAGRAM AND DOA ESTIMATION

The imaging performance is compared for the quasi-coherent and incoherent case using the range-velocity (R-v-) diagram and the DoA estimation. The measurement results shown in Fig. 10 are performed by a measurement setup as in Fig. 5(a)

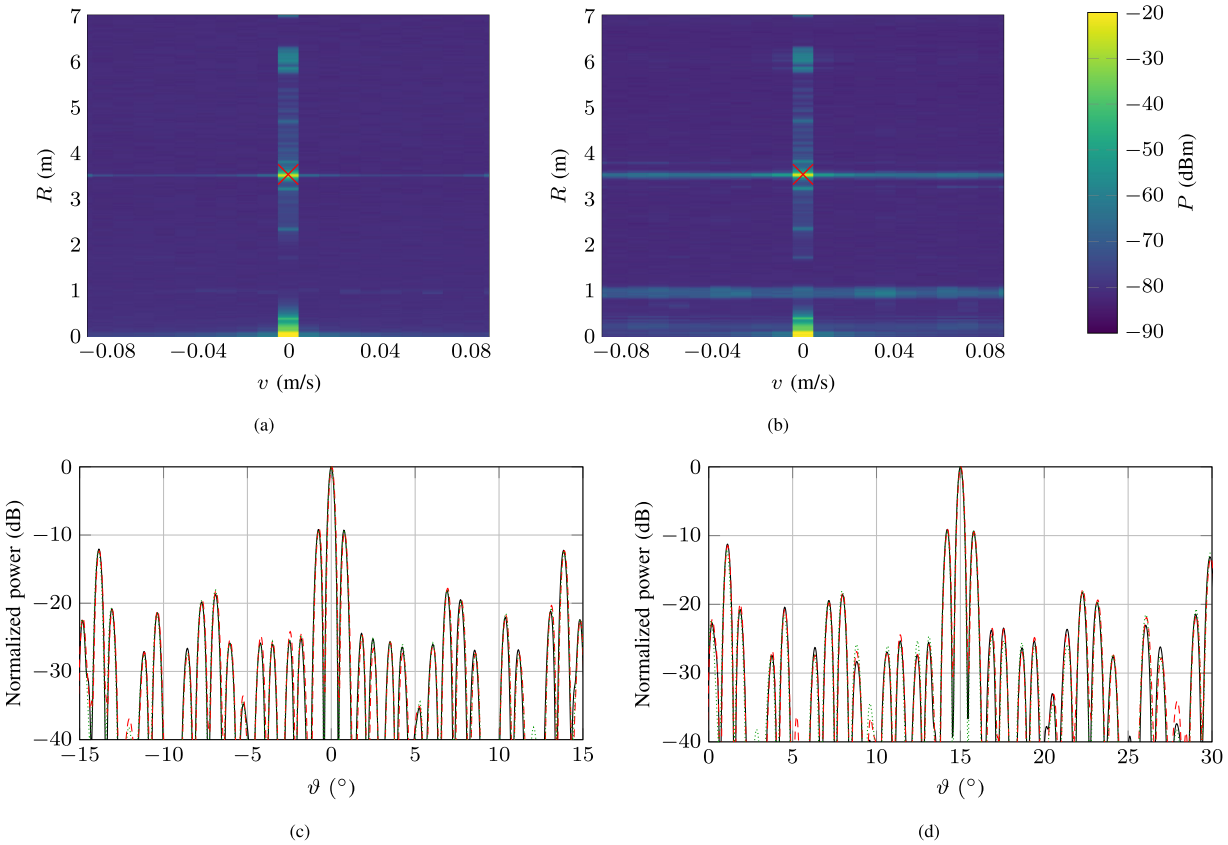

FIGURE 10. Imaging performance of the multistatic MIMO radar network. R-v-diagram of (a) the quasi-coherent and (b) the incoherent setup. DoA estimation for a radar target located at (c) the incident angle $\vartheta = 0$ and (d) the incident angle $\vartheta = 15°$ with quasi-coherent (——) and incoherent (- - -) signal synthesis in comparison to the simulation of the coherent case (·····).

for a target at the distance $R = 3.5\,\text{m}$ and an incident angle $\vartheta = 15°$. Since the same detection performance can be achieved in monostatic and bistatic radar responses (see Section IV-IV-B) for both the quasi-coherent and incoherent case when using the DDS with DRO, the resulting noise level is the same in both cases and in accordance with the thermal noise level. For the incoherent case, the phase stability between successive ramps is dependent on the frequency and phase correction for each ramp [13]. As the accuracy of the estimated correction value also depends on the low SNR of the reference target, the phase trend between successive ramps is not perfectly constant and superimposed by noise. This results in an increased sidelobe level in the velocity domain. For moving targets, the phase trend between successive ramps changes linearly. Due to the same correction as for static targets, this linear phase trend is also superimposed by noise. This results in the same increased sidelobe level as for static targets. Nevertheless, the correct determination of the velocity of the target is not affected by this correction. The phase stability between successive radar measurements is sufficiently large to lead to the same DoA estimation performance for both non-coherent systems (see Fig. 10(c) and (d)).

V. CONCLUSION

In this article, a phase noise analysis regarding the achievable detection and imaging performance of non-coherent (quasi-coherent and incoherent) multistatic MIMO radar networks is given when using the DDS and the PLL as frequency synthesizers. The multistatic radar network consists of multiple radar sensor nodes with an individual signal synthesizer for each node. It is shown that the hardware architecture of a DDS is beneficial for bistatic signal paths, as the phase noise of the DDS is only determined by the very low internal phase noise of the DDS circuit and the reference oscillator. In case of the PLL, also the VCO and the LF have to be considered as they have a major influence on the output phase noise. It is shown that the use of a common reference oscillator (quasi-coherent system) reduces the hardware effort compared to a fully coherent system and relaxes the requirement for the quality of the used reference oscillator. Measurements with a multistatic MIMO radar at 150 GHz prove that by using the DDS, it is possible to achieve the same detection and imaging performance as for a coherent system, although the signals are generated in a quasi-coherent or incoherent system configuration.

REFERENCES

[1] C. Waldschmidt, J. Hasch, and W. Menzel, "Automotive radar – From first efforts to future systems," *IEEE J. Microwaves*, vol. 1, no. 1, pp. 135–148, Jan. 2021.

[2] D. Zankl *et al.*, "BLASTDAR — A large radar sensor array system for blast furnace burden surface imaging," *IEEE Sensors J.*, vol. 15, no. 10, pp. 5893–5909, Oct. 2015.

[3] J. Lien *et al.*, "Soli: Ubiquitous gesture sensing with millimeter wave radar," *ACM Trans. Graph.*, vol. 35, no. 4, pp. 1–19, Jul. 2016.

[4] M. Skolnik, G. Linde, and K. Meads, "Senrad: An advanced wideband air-surveillance radar," *IEEE Trans. Aerosp. Electron. Syst.*, vol. 37, no. 4, pp. 1163–1175, Oct. 2001.

[5] S. S. Ahmed, A. Genghammer, A. Schiessl, and L. Schmidt, "Fully electronic *E*-band personnel imager of 2 m^2 aperture based on a multistatic architecture," *IEEE Trans. Microw. Theory Techn.*, vol. 61, no. 1, pp. 651–657, Jan. 2013.

[6] T. Spreng, S. Yuan, V. Valenta, H. Schumacher, U. Siart, and V. Ziegler, "Wideband 120 GHz to 140 GHz MIMO radar: System design and imaging results," in *Proc. Eur. Microw. Conf.*, 2015, pp. 430–433.

[7] A. Dürr *et al.*, "High-resolution 160-GHz imaging MIMO radar using MMICs with on-chip frequency synthesizers," *IEEE Trans. Microw. Theory Techn.*, vol. 67, no. 9, pp. 3897–3907, Sep. 2019.

[8] Texas Instruments, "AWR2243 single-chip 76- to 81-GHz FMCW transceiver," *Data Sheet*, Aug. 2020. Accessed: Dec. 2021. [Online]. Available: https://www.ti.com/product/AWR2243

[9] S. Kueppers, H. Cetinkaya, R. Herschel, and N. Pohl, "A compact 24 × 24 channel MIMO FMCW radar system using a substrate integrated waveguide-based reference distribution backplane," *IEEE Trans. Microw. Theory Techn.*, vol. 68, no. 6, pp. 2124–2133, Apr. 2020.

[10] M. C. Budge and M. P. Burt, "Range correlation effects in radars," in *Proc. Rec. IEEE Nat. Radar Conf.*, 1993, pp. 212–216.

[11] A. Frischen, J. Hasch, and C. Waldschmidt, "A cooperative MIMO radar network using highly integrated FMCW radar sensors," *IEEE Trans. Microw. Theory Techn.*, vol. 65, no. 4, pp. 1355–1366, Apr. 2017.

[12] A. Dürr, B. Schneele, D. Schwarz, and C. Waldschmidt, "Range-angle coupling and near-field effects of very large arrays in mm-wave imaging radars," *IEEE Trans. Microw. Theory Techn.*, vol. 69, no. 1, pp. 262–270, Sep. 2021.

[13] A. Dürr, R. Kramer, D. Schwarz, M. Geiger, and C. Waldschmidt, "Calibration-based phase coherence of incoherent and quasi-coherent 160-GHz MIMO radars," *IEEE Trans. Microw. Theory Techn.*, vol. 68, no. 7, pp. 2768–2778, Apr. 2020.

[14] M. Gottinger, F. Kirsch, P. Gulden, and M. Vossiek, "Coherent full-duplex double-sided two-way ranging and velocity measurement between separate incoherent radio units," *IEEE Trans. Microw. Theory Techn.*, vol. 67, no. 5, pp. 2045–2061, May 2019.

[15] M. Steiner, T. Grebner, and C. Waldschmidt, "Chirp-sequence-based imaging using a network of distributed single-channel radar sensors," in *Proc. IEEE MTT-S Int. Conf. Microw. Intell. Mobility*, 2019, pp. 1–4.

[16] A. M. Haimovich, R. S. Blum, and L. J. Cimini, "MIMO radar with widely separated antennas," *IEEE Signal Process. Mag.*, vol. 25, no. 1, pp. 116–129, Dec. 2008.

[17] S. Roehr, P. Gulden, and M. Vossiek, "Method for high precision clock synchronization in wireless systems with application to radio navigation," in *Proc. IEEE Radio Wireless Symp.*, 2007, pp. 551–554.

[18] S. Roehr, P. Gulden, and M. Vossiek, "Precise distance and velocity measurement for real time locating in multipath environments using a frequency-modulated continuous-wave secondary radar approach," *IEEE Trans. Microw. Theory Techn.*, vol. 56, no. 10, pp. 2329–2339, Oct. 2008.

[19] A. Frischen, J. Hasch, and C. Waldschmidt, "Performance degradation in cooperative radar sensor systems due to uncorrelated phase noise," in *Proc. 11th Eur. Radar Conf.*, 2014, pp. 241–244.

[20] A. Frischen, J. Hasch, and C. Waldschmidt, "Contour recognition with a cooperative distributed radar sensor network," in *Proc. Microw. Intell. Mobility*, 2015, pp. 1–4.

[21] M. Gottinger *et al.*, "Coherent automotive radar networks: The next generation of radar-based imaging and mapping," *IEEE J. Microwaves*, vol. 1, no. 1, pp. 149–163, Jan. 2021.

[22] M. Gottinger, P. Gulden, and M. Vossiek, "Coherent signal processing for loosely coupled bistatic radar," *IEEE Trans. Aerosp. Electron. Syst.*, vol. 57, no. 3, pp. 1855–1871, Jun. 2021.

[23] G. Rubio-Cidre, A. Badolato, L. Úbeda Medina, J. Grajal, B. Mencia-Oliva, and B.-P. Dorta-Naranjo, "DDS-based signal-generation architecture comparison for an imaging radar at 300 GHz," *IEEE Trans. Instrum. Meas.*, vol. 64, no. 11, pp. 3085–3098, Nov. 2015.

[24] A. Dürr *et al.*, "On the calibration of mm-wave MIMO radars using sparse antenna arrays for DoA estimation," in *Proc. Eur. Radar Conf.*, 2019, pp. 349–352.

[25] J. A. Crawford, *Frequency Synthesizer Design Handbook*. Norwood, MA, USA: Artech House, Jun. 1994.

[26] D. Banerjee, *PLL Performance, Simulation, and Design*, 4th ed. Indianapolis, IN, USA: Dog Ear, 2006.

[27] M. Pichler, A. Stelzer, P. Gulden, C. Seisenberger, and M. Vossiek, "Phase-error measurement and compensation in PLL frequency synthesizers for FMCW Sensors-I: Context and application," *IEEE Trans. Circuits Syst. I, Reg. Papers*, vol. 54, no. 5, pp. 1006–1017, May 2007.

[28] M. Pichler, A. Stelzer, P. Gulden, C. Seisenberger, and M. Vossiek, "Phase-error measurement and compensation in PLL frequency synthesizers for FMCW Sensors-II: Theory," *IEEE Trans. Circuits Syst. I, Reg. Papers*, vol. 54, no. 6, pp. 1224–1235, Jun. 2007.

[29] H. Arora, N. Klemmer, J. C. Morizio, and P. D. Wolf, "Enhanced phase noise modeling of fractional-N frequency synthesizers," *IEEE Trans. Circuits Syst. I, Reg. Papers*, vol. 52, no. 2, pp. 379–395, Feb. 2005.

[30] A. Stelzer, E. Kolmhofer, and S. Scheiblhofer, "Fast 77 GHz chirps with direct digital synthesis and phase locked loop," in *Asia-Pacific Microw. Conf. Proc.*, 2005.

[31] J. Vankka, J. Lindeberg, and K. Halonen, "Direct digital synthesizer with tunable phase and amplitude error feedback structures," in *Proc. Int. Symp. Circuits Syst.*, 2003.

[32] V. V. Romashov, L. V. Romashova, and K. K. Khramov, "Research of phase noise of direct digital synthesizers," in *Proc. Int. Siberian Conf. Control Commun.*, 2011, pp. 168–171.

[33] K. V. Puglia, "Phase noise analysis of component cascades," *IEEE Microw. Mag.*, vol. 3, no. 4, pp. 71–75, Dec. 2002.

[34] M. I. Skolnik, *Introduction to Radar Systems (Electrical Engineering Series)*, 3rd ed. New York, NY, USA: McGraw-Hill, 2001.

[35] K. Thurn, R. Ebelt, and M. Vossiek, "Noise in homodyne FMCW radar systems and its effects on ranging precision," in *IEEE MTT-S Int. Microw. Symp. Dig.*, 2013, pp. 1–3.

[36] W. Kester *et al.*, *Data Conversion Handbook (Analog Devices Series)*. London, U.K.: Newnes, Dec. 2004.

[37] A. Dürr, D. Schwarz, and C. Waldschmidt, "A system analysis of noise influences on the imaging performance of millimeter wave MIMO radars," in *Proc. IEEE/MTT-S Int. Microw. Symp.*, 2020, pp. 1019–1022.

[38] M. Hitzler, P. Grüner, L. Boehm, W. Mayer, and C. Waldschmidt, "On monostatic and bistatic system concepts for mm-wave radar MMICs," *IEEE Trans. Microw. Theory Techn.*, vol. 66, no. 9, pp. 4204–4215, Sep. 2018.

ANDRÉ DÜRR (Graduate Student Member, IEEE) received the M.Sc. degree in 2017 from Ulm University, Ulm, Germany, where he is currently working toward the Ph.D. degree.

From 2015 to 2016, he was an Intern with Bosch Research and Technology Center North America, Palo Alto, CA, USA. In 2017, he joined the Institute of Microwave Engineering, Ulm University. His research interests include novel imaging radar sensor concepts, phase noise mitigation, and performance degradation of noncoherent multichannel radar systems and their synchronization, all at millimeter-wave frequencies.

Mr. Dürr was the recipient of the Argus Science Award in 2015, Verband der Elektrotechnik Elektronik Informationstechnik (VDE) Award in 2015, and Verband Deutscher Ingenieure (VDI) Award in 2017.

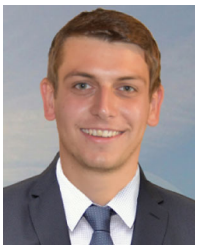

DENNIS BÖHM received the M.Sc. degree from Ulm University, Ulm, Germany, in 2021.

From 2018 to 2021, he was a Student Trainee with Hensoldt Sensors, Ulm, Germany, where he was working in the field of transmit and receive modules. In 2021, he joined Hensoldt Sensors, where he is currently working on radar front ends and related high frequency measurements.

Mr. Böhm was the recipient of the Argus Science Award in 2018.

DOMINIK SCHWARZ (Graduate Student Member, IEEE) received the M.Sc. degree in 2018 from Ulm University, Ulm, Germany, where he is currently working toward the Ph.D. degree.

From 2011 to 2018, he was a Student Trainee with Hensoldt Sensors, Ulm, Germany. In 2018, he joined the Institute of Microwave Engineering, Ulm University. His research interests include automotive MIMO radars with a focus on high bandwidths, high channel counts, 2D-DoA estimation, and novel multilayer PCB structures at millimeter-wave frequencies.

Mr. Schwarz was the recipient of the Ingenieure for Kommunikation (IfKom) Award in 2016 and Argus Science Award in 2019.

STEPHAN HÄFNER received the M.Sc. degree in computer engineering and the Dr.-Ing. (Ph.D.E.E.) degree from the Technische Universität Ilmenau, Ilmenau, Germany, in 2012 and 2021, respectively.

Since 2012, he has been with the Electronic Measurement Research Laboratory (now Electronic Measurements and Signal Processing Group), Technische Universität Ilmenau. His research interests include high-resolution parameter estimation for channel sounding and radar applications.

REINER THOMÄ (Fellow, IEEE) received the Dipl.-Ing. (M.S.E.E.), Dr.-Ing. (Ph.D.E.E.), and the Dr.-Ing. habil. degrees in electrical engineering and information technology from Technische Hochschule Ilmenau, Ilmenau, Germany, in 1975, 1983, and 1989, respectively.

From 1975 to 1988, he was a Research Associate in the fields of electronic circuits, measurement engineering, and digital signal processing at the same university. From 1988 to 1990, he was a Research Engineer with Akademie der Wissenschaften der DDR (Zentrum för Wissenschaftlichen Gerätebau). During this period, he was working in the field of radio surveillance. In 1991, he spent a sabbatical leave with the University of Erlangen-Nörnberg (Lehrstuhl för Nachrichtentechnik), Erlangen, Germany. Since 1992, he has been a Professor of electrical engineering (electronic measurement) with TU Ilmenau, Ilmenau, Germany, where he was the Director of the Institute of Communications and Measurement Engineering from 1999 to 2005. With his group, he has contributed to several European and German research projects and clusters, such as RESCUE, WINNER, PULSERS, EUWB, NEWCOM, COST 273, COST 2100, IC 1004, IRACON, EASY-A, and EASY-C. He was the Speaker of the German nation-wide DFG-focus project UKoLOS, Ultra-Wideband Radio Technologies for Communications, Localization, and Sensor Applications (SPP 1202). He became an Advisory Board Member of EU project mmMAGIC. His research interests include measurement and digital signal processing methods (correlation and spectral analysis, system identification, sensor arrays, compressive sensing, time-frequency and cyclostationary signal analysis), their application in mobile radio and radar systems (multidimensional channel sounding, propagation measurement and parameter estimation, MIMO-, mm-wave-, and ultra-wideband radar), measurement-based performance evaluation of MIMO transmission systems, including over-the-air testing in virtual electromagnetic environments, passive coherent location, and UWB radar sensor systems for object detection, tracking and imaging.

Dr. Thomä is a member of URSI (Comm. A) and VDE/ITG. Since 1999, he has been the Chair of the IEEE-IM TC-13 on Measurement in Wireless and Telecommunications. In 2007, he was awarded IEEE Fellow and was the recipient of the Thuringian State Research Award for Applied Research, both for contributions to high-resolution multidimensional channel sounding. In 2014, he was the recipient of the Vodafone Innovation Award.

CHRISTIAN WALDSCHMIDT (Fellow, IEEE) received the Dipl.-Ing. (M.S.E.E.) and the Dr.-Ing. (Ph.D.E.E.) degrees from University Karlsruhe (TH), Karlsruhe, Germany, in 2001 and 2004, respectively.

From 2001 to 2004, he was a Research Assistant with the Institut för Höchstfrequenztechnik and Elektronik, TH. Since 2004, he has been with Robert Bosch GmbH in the business units Corporate Research and Chassis Systems. He was heading different research and development teams in microwave engineering, RF-sensing, and automotive radar. In 2013, he returned to academia and was appointed as the Director of the Institute of Microwave Engineering, University Ulm, Ulm, Germany, as Full Professor. He authored or coauthored more than 200 scientific publications and more than 20 patents. His research interests include radar and RF-sensing, mm-wave and submillimeter-wave engineering, antennas and antenna arrays, and RF and array signal processing.

Dr. Waldschmidt is a member of the Executive Committee Board of the German MTT/AP Joint Chapter and a member of the German Information Technology Society (ITG). He was the Chair of the IEEE MTT-27 Technical Committee on wireless enabled automotive and vehicular applications. He was the two-time TPC Chair and General Chair of the IEEE MTT International Conference on Microwaves for Intelligent Mobility. Since 2018, he has been an Associate Editor for IEEE MICROWAVE WIRELESS COMPONENTS LETTERS. He is a reviewer of multiple IEEE transactions and many IEEE conferences in the field of microwaves. He has been the co-recipient of 11 best paper awards since 2014.